


Temperature Dependent Resistivity of Chiral Single-Walled Carbon Nanotubes in the Presence of Coherent Light Source

Anthony Twum^{1*} , Raymond Edziah¹, Samuel Yeboah Mensah¹, Kwadwo Dompseh¹, Patrick Mensah-Amoah¹, Augustine Arthur¹, Natalia G. Mensah², Kofi Adu³, George Nkrumah-Buandoh⁴

¹Department of Physics, University of Cape Coast, Cape Coast, Ghana

²Department of Mathematics, University of Cape Coast, Cape Coast, Ghana

³Department of Physics, The Pennsylvania State University-Altoona College, Altoona, USA

⁴Department of Physics, University of Ghana, Accra, Ghana

Email: *atwum@ucc.edu.gh

How to cite this paper: Twum, A., Edziah, R., Mensah, S.Y., Dompseh, K., Mensah-Amoah, P., Arthur, A., Mensah, N.G., Adu, K. and Nkrumah-Buandoh, G. (2021) Temperature Dependent Resistivity of Chiral Single-Walled Carbon Nanotubes in the Presence of Coherent Light Source. *World Journal of Condensed Matter Physics*, 11, 77-86.

<https://doi.org/10.4236/wjcmp.2021.114006>

Received: October 18, 2021

Accepted: November 27, 2021

Published: November 30, 2021

Copyright © 2021 by author(s) and Scientific Research Publishing Inc.

This work is licensed under the Creative Commons Attribution International License (CC BY 4.0).

<http://creativecommons.org/licenses/by/4.0/>



Open Access

Abstract

We have studied the axial resistivity of chiral single-walled carbon nanotubes (SWCNTs) in the presence of a combined direct current and high frequency alternating fields. We employed semiclassical Boltzmann equations approach and compared our results with a similar study that examined the circumferential resistivity of these unique materials. Our work shows that these materials display similar resistivity for both axial and circumferential directions and this largely depends on temperature, intensities of the applied fields and material parameters such as chiral angle. Based on these low-temperature bi-directional conductivity responses, we propose chiral SWCNTs for design of efficient optoelectronic devices.

Keywords

Chiral Single-Wall Carbon Nanotubes, Boltzmann Transport Equation, Axial Resistivity, Chiral Angle

1. Introduction

Since the accidental discovery of carbon nanotubes (CNTs) and their fabrication by Iijima in the early 1990s [1], there has been a lot of research interest in this novel material. Several research works have reported practical usefulness of CNTs as composites, catalysts and molecular wires. Essentially, CNTs are tiny and single sheets of carbon atom rolled into seamlessly meshed tubes at the nanoscale

level [2]. The unique material properties of CNTs are their characteristic electrical and thermal conductivities. A CNT is either single-walled or multi-walled. Single-walled carbon nanotubes (SWCNTs) consist of a roll of one graphene sheet. The electrical behaviour of SWCNTs is determined by their chirality [3]. Researchers in [4] studied the electrical behaviour of multi-walled carbon nanotubes (MWCNTs) network embedded in amorphous silicon nitride. As part of their findings, they reported that the resistance-temperature characteristic is practically linear except at very low temperatures. This suggests a metallic behaviour of the MWCNT networks. Experimental investigations have also been carried out on the scaling of resistance and electron mean-free-path of SWCNTs [5]. Furthermore, the authors in [5] determined the length-dependent resistance of SWCNTs and also considered the variation of resistivity with temperature. The temperature dependent resistivity of armchair CNTs has also been studied experimentally [6] and the results clearly indicated metallic behavior of the SWCNT at high temperatures with resistivity increasing approximately linearly with temperature.

In this paper, we studied the temperature dependent resistivity of SWCNTs along their tubular axes in the presence of a combined direct current and laser radiation. Our results are compared with similar findings reported in reference [7] which reported on resistivity of these novel materials along the base helix.

2. Theory

Using semi-classical Boltzmann transport equation (BTE) with constant electron relaxation time, the carrier current density and axial resistivity in the SWCNT is evaluated as functions of the geometric chiral angle θ_b , temperature T , the real overlapping integrals for jumps along the nanotube axis Δ_z and the base helix Δ_s . This is done by following the approach of [7] [8] together with the phenomenological model of a SWCNT developed in references [9] [10]. Employing BTE, a chiral SWCNT placed in an electric field applied along the nanotube axis studied under a temperature gradient ∇T such that

$$\frac{\partial f(r, p, t)}{\partial t} + v(p) \frac{\partial f(r, p, t)}{\partial r} + eE(t) \frac{\partial f(r, p, t)}{\partial p} = -\frac{f(r, p, t) - f_0(p)}{\tau} \quad (1)$$

where $f(r, p, t)$ is the distribution function, $f_0(p)$ is the equilibrium distribution function, $v(p)$ is the electron velocity, r is the electron position, p is the electron dynamical momentum, t is time elapsed, τ is the electron relaxation time which is assumed to be constant and e is the electron charge. The applied dc-ac field, $E(t) = E_0 + E_1 \cos(wt)$, where E_0 is the constant electric field, E_1 and w are the amplitude and frequency of the ac field, respectively.

We employ the perturbation approach to solve Equation (1) by treating the second term on the left-hand side as a weak perturbation. In the linear approximation of ∇T and $\nabla \mu$, the solution to Equation (1) is

$$f(p) = \tau^{-1} \int_0^\infty \exp\left(-\frac{t}{\tau}\right) f_0\left(p - e \int_{t-t'}^t [E_0 + E_1 \cos wt'] dt'\right) dt$$

$$\begin{aligned}
& + \int_0^\infty \exp\left(-\frac{t}{\tau}\right) dt \left\{ \left[\varepsilon\left(p - e \int_{t-t'}^t [E_0 + E_1 \cos wt'] dt'\right) - \mu \right] \frac{\nabla T}{T} + \nabla \mu \right\} \\
& \times v\left(p - e \int_{t-t'}^t [E_0 + E_1 \cos wt'] dt'\right) \frac{\partial f_0}{\partial \varepsilon}\left(p - e \int_{t-t'}^t [E_0 + E_1 \cos wt'] dt'\right)
\end{aligned} \quad (2)$$

where $\varepsilon(p)$ is the tight-binding energy of the electron and μ is the chemical potential.

The current density is expressed as

$$j = e \sum_p v(p) f(p) \quad (3)$$

Substituting Equation (2) into Equation (3) gives

$$\begin{aligned}
j & = e \tau^{-1} \int_0^\infty \exp\left(-\frac{t}{\tau}\right) dt \sum_p v(p) f_0\left(p - e \int_{t-t'}^t [E_0 + E_1 \cos wt'] dt'\right) \\
& + e \int_0^\infty \exp\left(-\frac{t}{\tau}\right) dt \sum_p v(p) \left\{ \left[\varepsilon\left(p - e \int_{t-t'}^t [E_0 + E_1 \cos wt'] dt'\right) - \mu \right] \frac{\nabla T}{T} + \nabla \mu \right\} \\
& \times v\left(p - e \int_{t-t'}^t [E_0 + E_1 \cos wt'] dt'\right) \frac{\partial f_0}{\partial \varepsilon}\left(p - e \int_{t-t'}^t [E_0 + E_1 \cos wt'] dt'\right)
\end{aligned} \quad (4)$$

Employing the transformation

$$p - e \int_{t-t'}^t [E_0 + E_1 \cos wt'] dt' \rightarrow p,$$

Equation (4) becomes

$$\begin{aligned}
j & = e \tau^{-1} \int_0^\infty \exp\left(-\frac{t}{\tau}\right) dt \sum_p v\left(p - e \int_{t-t'}^t [E_0 + E_1 \cos wt'] dt'\right) f_0(p) \\
& + e \int_0^\infty \exp\left(-\frac{t}{\tau}\right) dt \sum_p \left\{ \left[\varepsilon(p) - \mu \right] \frac{\nabla T}{T} + \nabla \mu \right\} \\
& \times \left\{ v(p) \frac{\partial f_0(p)}{\partial \varepsilon} \right\} v\left(p - e \int_{t-t'}^t [E_0 + E_1 \cos wt'] dt'\right)
\end{aligned} \quad (5)$$

We employ the phenomenological approach of references [9] [10] by considering a SWCNT as an infinitely long periodic chain of carbon atoms wrapped along a base helix. The axial current density is decomposed into the form

$$j_z = Z' + Y' \sin \theta_h \quad (6)$$

where Z and Y are components of the current density along the nanotube axis and the base helix, respectively.

Furthermore, we neglect the interference between the axial and helical paths connecting a pair of atoms, quantization of transverse motion can be ignored [9] [10]; an approximation that best describes doped chiral carbon nanotubes [11].

Resolving the current density along the tubular axis (z-axis) and base helix, we obtain

$$\begin{aligned}
Z' & = e \tau^{-1} \int_0^\infty \exp\left(-\frac{t}{\tau}\right) dt \sum_p v_z\left(p - e \int_{t-t'}^t [E_0 + E_1 \cos wt'] dt'\right) f_0(p) \\
& + e \int_0^\infty \exp\left(-\frac{t}{\tau}\right) dt \sum_p \left\{ \left[\varepsilon(p) - \mu \right] \frac{\nabla_z T}{T} + \nabla_z \mu \right\}
\end{aligned}$$

$$\times \left\{ v_z(p) \frac{\partial f_0(p)}{\partial \varepsilon} \right\} v_z \left(p - e \int_{t-t'}^t [E_0 + E_1 \cos wt'] dt' \right) \quad (7)$$

and

$$Y' = e\tau^{-1} \int_0^\infty \exp\left(-\frac{t}{\tau}\right) dt \sum_p v_y \left(p - e \int_{t-t'}^t [E_0 + E_1 \cos wt'] dt' \right) f_0(p) + e \int_0^\infty \exp\left(-\frac{t}{\tau}\right) dt \sum_p \left\{ [\varepsilon(p) - \mu] \frac{\nabla_y T}{T} + \nabla_y \mu \right\} \times \left\{ v_y(p) \frac{\partial f_0(p)}{\partial \varepsilon} \right\} v_y \left(p - e \int_{t-t'}^t [E_0 + E_1 \cos wt'] dt' \right) \quad (8)$$

Equations (7) and (8) are transformed using

$$\sum_p \rightarrow \frac{2}{(2\pi\hbar)^2} \int_{-\frac{\pi}{d_y}}^{\frac{\pi}{d_y}} dp_y \int_{-\frac{\pi}{d_z}}^{\frac{\pi}{d_z}} dp_z$$

where d_z and d_y are the inter-atomic distance along the nanotube axis and the base helix respectively. Therefore, Z' and Y' become,

$$Z' = \frac{2e\tau^{-1}}{(2\pi\hbar)^2} \int_0^\infty \exp\left(-\frac{t}{\tau}\right) dt \int_{-\frac{\pi}{d_y}}^{\frac{\pi}{d_y}} dp_y \int_{-\frac{\pi}{d_z}}^{\frac{\pi}{d_z}} dp_z v_z \left(p - e \int_{t-t'}^t [E_0 + E_1 \cos wt'] dt' \right) f_0(p) + \frac{2e}{(2\pi\hbar)^2} \int_0^\infty \exp\left(-\frac{t}{\tau}\right) dt \int_{-\frac{\pi}{d_y}}^{\frac{\pi}{d_y}} dp_y \int_{-\frac{\pi}{d_z}}^{\frac{\pi}{d_z}} dp_z \left\{ [\varepsilon(p) - \mu] \frac{\nabla_z T}{T} + \nabla_z \mu \right\} \times \left\{ v_z(p) \frac{\partial f_0(p)}{\partial \varepsilon} \right\} v_z \left(p - e \int_{t-t'}^t [E_0 + E_1 \cos wt'] dt' \right) \quad (9)$$

and

$$Y' = \frac{2e\tau^{-1}}{(2\pi\hbar)^2} \int_0^\infty \exp\left(-\frac{t}{\tau}\right) dt \int_{-\frac{\pi}{d_y}}^{\frac{\pi}{d_y}} dp_y \int_{-\frac{\pi}{d_z}}^{\frac{\pi}{d_z}} dp_z v_y \left(p - e \int_{t-t'}^t [E_0 + E_1 \cos wt'] dt' \right) f_0(p) + \frac{2e}{(2\pi\hbar)^2} \int_0^\infty \exp\left(-\frac{t}{\tau}\right) dt \int_{-\frac{\pi}{d_y}}^{\frac{\pi}{d_y}} dp_y \int_{-\frac{\pi}{d_z}}^{\frac{\pi}{d_z}} dp_z \left\{ [\varepsilon(p) - \mu] \frac{\nabla_y T}{T} + \nabla_y \mu \right\} \times \left\{ v_y(p) \frac{\partial f_0(p)}{\partial \varepsilon} \right\} v_y \left(p - e \int_{t-t'}^t [E_0 + E_1 \cos wt'] dt' \right) \quad (10)$$

The integrals in Equations (9) and (10) were evaluated over the first Brillouin zone. The parameters v , p , E , ∇T and $\nabla \mu$ with subscripts z and y represent the respective components along the nanotube axis and along the base helix.

The energy dispersion relation for a chiral nanotube obtained in the tight-binding approximation is expressed as:

$$\varepsilon(p) = \varepsilon_0 - \Delta_y \cos \frac{p_y d_y}{\hbar} - \Delta_z \cos \frac{p_z d_z}{\hbar} \quad (11)$$

where ε_0 is the energy of an outer-shell electron in an isolated carbon atom, Δ_z and Δ_y are the real overlapping integrals for jumps along the respective coordinates, p_y and p_z are the components of momentum tangential to the base helix and along the nanotube axis, respectively. The components v_y and v_z of the electron velocity v are respectively,

$$v_y(p) = \frac{\partial \varepsilon(p)}{\partial P_y} = \frac{\Delta_y d_y}{\hbar} \sin \frac{p_y d_y}{\hbar} \quad (12)$$

$$v_z(p) = \frac{\partial \varepsilon(p)}{\partial P_z} = \frac{\Delta_z d_z}{\hbar} \sin \frac{p_z d_z}{\hbar} \quad (13)$$

Also,

$$\begin{aligned} & v_y \left(p - e \int_{t-t'}^t [E_0 + E_1 \cos wt'] dt' \right) \\ &= \frac{\partial \varepsilon}{\partial P_y} \left(p - e \int_{t-t'}^t [E_0 + E_1 \cos wt'] dt' \right) \\ &= \frac{\Delta_y d_y}{\hbar} \left\{ \sin \frac{p_y d_y}{\hbar} \cos \left(p - e \int_{t-t'}^t [E_0 + E_1 \cos wt'] dt' \right) \right. \\ &\quad \left. - \cos \frac{p_y d_y}{\hbar} \sin \left(p - e \int_{t-t'}^t [E_0 + E_1 \cos wt'] dt' \right) \right\} \end{aligned} \quad (14)$$

Similarly,

$$\begin{aligned} & v_z = \frac{\Delta_z d_z}{\hbar} \left\{ \sin \frac{p_z d_z}{\hbar} \cos \left(p - e \int_{t-t'}^t [E_0 + E_1 \cos wt'] dt' \right) \right. \\ &\quad \left. - \cos \frac{p_z d_z}{\hbar} \sin \left(p - e \int_{t-t'}^t [E_0 + E_1 \cos wt'] dt' \right) \right\} \end{aligned} \quad (15)$$

The carrier density of the non-degenerate electron gas can be determined by expressing the Boltzmann equilibrium distribution function $f_0(p)$ as

$$f_0(p) = C \exp \left(\frac{\Delta_y \cos \frac{p_y d_y}{\hbar} + \Delta_z \cos \frac{p_z d_z}{\hbar} + \mu - \varepsilon_0}{kT} \right) \quad (16)$$

The normalization constant C is expressed as

$$C = \frac{d_y d_z n_0}{2I_0(\Delta_y^*) I_0(\Delta_z^*)} \exp \left(-\frac{\mu - \varepsilon_0}{kT} \right)$$

where n_0 is the surface charge density, $I_n(x)$ is the modified Bessel function of n^{th} order,

$$\Delta_y^* = \frac{\Delta_y}{kT}, \quad \Delta_z^* = \frac{\Delta_z}{kT}$$

and k is Boltzmann's constant.

We substitute Equations (11)-(16) into Equations (9) and (10) and simplify the integrals to obtain

$$Y' = -\sigma_y(E) E_{ym}^* - \sigma_y(E) \frac{k}{e} \left\{ \left(\frac{\varepsilon_0 - \mu}{kT} \right) - \Delta_y^* \frac{I_0(\Delta_y^*)}{I_1(\Delta_y^*)} + 2 - \Delta_z^* \frac{I_1(\Delta_z^*)}{I_0(\Delta_z^*)} \right\} \nabla_y T \quad (17)$$

$$Z' = -\sigma_z(E)E_{zn}^* - \sigma_z(E) \frac{k}{e} \left\{ \left(\frac{\varepsilon_0 - \mu}{kT} \right) - \Delta_z^* \frac{I_0(\Delta_z^*)}{I_1(\Delta_z^*)} + 2 - \Delta_y^* \frac{I_1(\Delta_y^*)}{I_0(\Delta_y^*)} \right\} \nabla_z T \quad (18)$$

where we have defined E_{yn}^* as

$$E_{yn}^* = E_n + \nabla_y \frac{\mu}{e}, \quad E_{sn}^* = E_{zn}^* \sin \theta_h$$

Also, the electrical conductivity $\sigma_i(E)$ is expressed as

$$\sigma_i(E) = \frac{e^2 \tau \Delta_i d_i^2 n_0}{\hbar^2} \frac{I_1(\Delta_i^*)}{I_0(\Delta_i^*)} \sum_{n=-\infty}^{\infty} J_n^2(a) \left[\frac{1}{1 + \left(\frac{e d_i E_0}{\hbar} + n w \right)^2 \tau^2} \right], i = y, z \quad (19)$$

Substituting Equations (17) and (18) into Equation (6), we obtain the following expression for axial the current density as

$$\begin{aligned} j_z = & -\left\{ \sigma_z(E) + \sigma_y(E) \sin^2 \theta_h \right\} E_{zn}^* \\ & - \left\{ \sigma_z(E) \frac{k}{e} \left[\left(\frac{\varepsilon_0 - \mu}{kT} \right) - \Delta_z^* \frac{I_0(\Delta_z^*)}{I_1(\Delta_z^*)} + 2 - \Delta_y^* \frac{I_1(\Delta_y^*)}{I_0(\Delta_y^*)} \right] \right. \\ & \left. + \sigma_y(E) \frac{k}{e} \sin^2 \theta_h \left[\left(\frac{\varepsilon_0 - \mu}{kT} \right) - \Delta_y^* \frac{I_0(\Delta_y^*)}{I_1(\Delta_y^*)} + 2 - \Delta_z^* \frac{I_1(\Delta_z^*)}{I_0(\Delta_z^*)} \right] \right\} \nabla_z T \end{aligned} \quad (20)$$

Employing the following definitions

$$\xi = \frac{\varepsilon_0 - \mu}{kT}, \quad A_i = \frac{I_1(\Delta_i^*)}{I_0(\Delta_i^*)}, \quad B_i = \frac{I_0(\Delta_i^*)}{I_1(\Delta_i^*)} - \frac{2}{\Delta_i^*}, \quad i = y, z$$

Equation (20) becomes

$$\begin{aligned} j_z = & -\left\{ \sigma_z(E) + \sigma_y(E) \sin^2 \theta_h \right\} E_{zn}^* - \left\{ \sigma_z(E) \frac{k}{e} \left[\xi - \Delta_z^* B_z - \Delta_y^* A_y \right] \right. \\ & \left. + \sigma_y(E) \frac{k}{e} \sin^2 \theta_h \left[\xi - \Delta_y^* B_y - \Delta_z^* A_z \right] \right\} \nabla_z T \end{aligned} \quad (21)$$

Equation (21) defines the current density and the axial component of the electrical conductivity is the coefficient of the electric field E_{zn}^* given as

$$\sigma_{zz} = \sigma_z(E) + \sigma_y(E) \sin^2 \theta_h \quad (22)$$

The resistivity of the chiral SWCNT along its axial direction is defined as

$$\rho_z = \frac{1}{\sigma_z(E) + \sigma_y(E) \sin^2 \theta_h} \quad (23)$$

3. Results and Discussion

In this work, we employed BTE to analytically study the axial electrical resistivity of a chiral SWCNT and obtained an expression for the axial component of the electrical resistivity, ρ_z in the presence of applied field E as shown in Equation (23). The ρ_z expression was analyzed numerically by considering a chiral SWCNT

having the following parameters: $d_y = 1 \text{ \AA}$, $d_z = 2 \text{ \AA}$, $\tau = 0.3 \times 10^{-12} \text{ s}$ and $\theta_h = 4^\circ$, and $E_0 = 6.9063 \times 10^7 \text{ V/m}$, $w = 10^{12} \text{ s}^{-1}$ and $E_1 = 5 \times 10^7 \text{ V/m}$.

Figure 1(a) shows the dependence of the axial electrical resistivity, ρ_z on temperature T , for various fixed values of the d.c. field, E_0 . It is observed that at low temperatures up to about 100 K, ρ_z changes slowly with temperature and the temperature dependence of ρ_z becomes generally linear with increasing temperature. This observation is attributed to electron-phonon interactions which cause scattering of the charge carriers along the tubular axis of the chiral SWCNT as temperature increases. The relatively low values of resistivity of SWCNT observed in **Figure 1** clearly suggest that chiral SWCNTs do exhibit metallic properties. As observed in the case of circumferential resistivity [7], our results similarly reveal that as the electric field strength, E_0 increases the axial resistivity increases significantly. This temperature dependence resistivity response of SWCNTs has been observed experimentally [6] [12] [13]. This behaviour can be explained based on the fact that as E_0 is increased, the carbon atoms forming the walls of the SWCNT become more energized and tend to vibrate faster at larger amplitudes resulting in enhanced scattering of the electrons. Our study has also revealed that the resistivity of the SWCNTs decreases markedly with increasing Δ_y as shown in **Figure 1(b)**.

Figure 2 shows the variation of the axial current density with temperature for selected values of the chiral angle, θ_h and dimensionless parameter Δ_z . Increasing θ_h results in a decrease of the resistivity of the chiral SWCNT as seen in **Figure 2(a)**, a behaviour similar to that observed for **Figure 2(a)** reveals that increasing the chiral angle, θ_h results in a decrease of the resistivity of the chiral SWCNT. On the other hand, **Figure 2(b)** shows that keeping Δ_y constant and varying Δ_z decreases ρ_z by an order of magnitude. Also observed in **Figure 2(b)** is that ρ_z remains unchanged for all values of Δ_z at temperatures below 100 K but decreases steadily by small margins with increasing temperature.

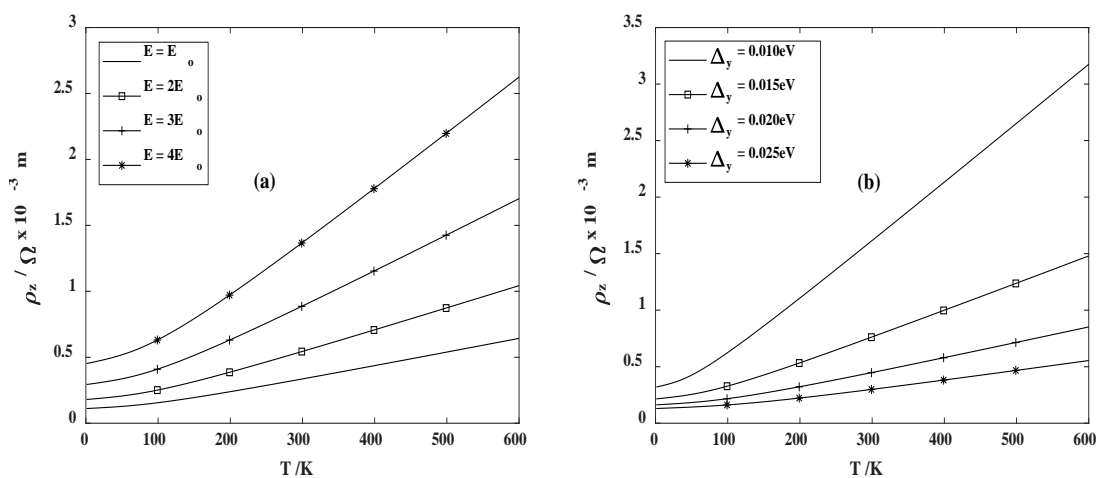


Figure 1. Dependence of axial current density (ρ_z) on temperature (T) for: (a) fixed values of the d.c. field E_0 , $2E_0$, $3E_0$ and $4E_0$, where $E_0 = 6.9063 \times 10^7 \text{ V/m}$, $E_1 = 5.0 \times 10^7 \text{ V/m}$, $\Delta_y = 0.018 \text{ eV}$ and $\Delta_z = 0.024 \text{ eV}$. (b) Fixed values of Δ_y , $\Delta_z = 0.024 \text{ eV}$, $E_1 = 5.0 \times 10^7 \text{ V/m}$, $E = 2E_0$, where $E_0 = 6.9063 \times 10^7 \text{ V/m}$.

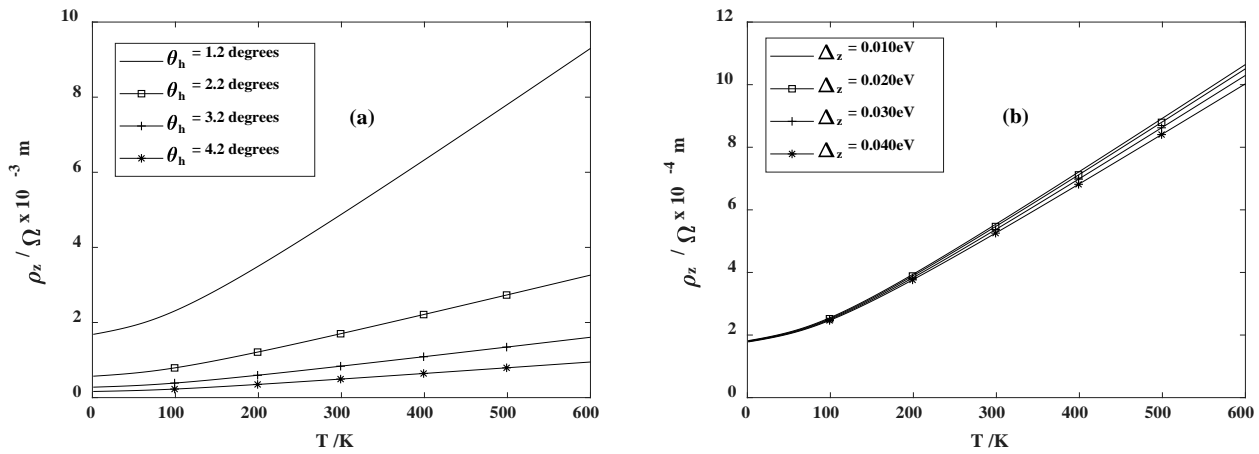


Figure 2. Variation of ρ_z with temperature for (a) fixed values of chiral angle, θ_h . $\Delta_z = 0.024$ eV, $\Delta_y = 0.018$ eV, $E_1 = 5.0 \times 10^7$ V/m, $E = 2E_0$, where $E_0 = 6.9063 \times 10^7$ V/m. (b) The dependence of ρ_z on temperature for various fixed values of Δ_z . $\Delta_y = 0.018$ eV, $E_1 = 5.0 \times 10^7$ V/m and $E = 2E_0$, where $E_0 = 6.9063 \times 10^7$ V/m.

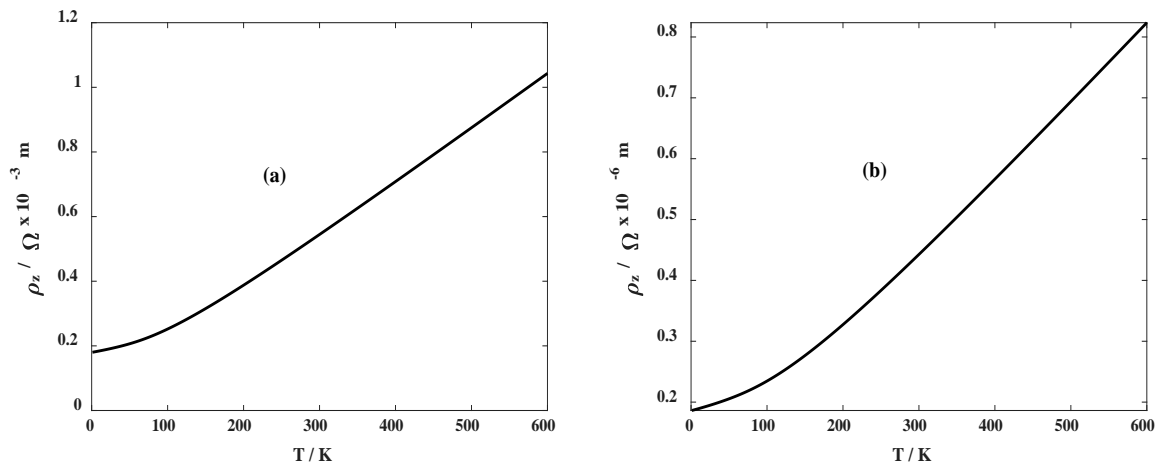


Figure 3. The dependence of ρ_z on temperature T for $\Delta_y = 0.018$ eV, $\Delta_z = 0.024$ eV, $E_1 = 5.0 \times 10^7$ V/m, $E = 2E_0$, where $E_0 = 6.9063 \times 10^7$ V/m, and chiral angle, $\theta_h = 4.0^\circ$ for the case in which (a) laser is turned and (b) laser is turned off.

On the other hand, when the a.c. source is switched off, $E_1 = 0$, $a = 0$, $w = 0$ and $J_n^2(a)$ becomes unity and equation (19) reduces to

$$\sigma_i(E) = \frac{e^2 \tau \Delta_i d_i^2 n_0}{\hbar^2} \frac{I_1(\Delta_i^*)}{I_0(\Delta_i^*)} \sum_{n=-\infty}^{\infty} J_n^2(a) \left[\frac{1}{1 + \left(\frac{e d_i E_0}{\hbar} \right)^2 \tau^2} \right], i = y, z$$

Figure 3 shows the dependence of axial resistivity of the chiral SWCNTs on temperature in the presence and absence of a laser. Clearly, when the laser source is switched off, ρ_z decreases by three orders of magnitude. This indicates that within the temperature range under consideration, the laser field modulates the d. c. field and enhances the momentum and kinetic energy of those electrons which are deficient in energy.

4. Conclusion

Using the semi-classical approach, the axial resistivity of a chiral SWCNT induced by a laser field has been investigated and compared with an earlier work that examined the circumferential resistivity of these unique materials. Our results indicate that the conductivity of SWCNTs is similar for both directions and is significantly influenced by material parameters (Δ_y , Δ_z , θ_h), the strengths of the constant field E_0 and laser source strength E_l . The axial resistivity can be increased by increasing the d.c. field strength and decreasing the chiral angle. As observed for the circumferential case, the axial resistivity also steadily and linearly increases with the chiral angle θ_h and real overlapping integral along the axial direction Δ_y at room temperatures. Therefore, SWCNTs can be used in the design of efficient optoelectronic devices.

Conflicts of Interest

The authors declare no conflicts of interest regarding the publication of this paper.

References

- [1] Iijima, S., Ajayan, P.M. and Ichihashi, T. (1992) Growth Model for Carbon Nanotubes. *Physical Review Letters*, **69**, 3100. <https://doi.org/10.1103/PhysRevLett.69.3100>
- [2] Zhou, W.Y., Bai, X.D., Wang, E.E. and Xie, S.S. (2009) Synthesis, Structure, and Properties of Single-Walled Carbon Nanotubes. *Advanced Materials*, **21**, 4565-4583. <https://doi.org/10.1002/adma.200901071>
- [3] Dekker, C. (1999) Carbon Nanotubes as Molecular Quantum Wires. *Physics Today*, **52**, 22-30. <https://doi.org/10.1063/1.882658>
- [4] Ionel, S., Lepadatu, A.-M., Teodorescu, V.S., Ciurea, M.L., Iancu, V., Dragoman, M., Konstantinidis, G. and Buiculescu, R. (2011) Electrical Behavior of Multi-Walled Carbon Nanotube Network Embedded in Amorphous Silicon Nitride. *Nanoscale Research Letters*, **6**, Article Number: 88. <https://doi.org/10.1186/1556-276X-6-88>
- [5] Purewal, M.S., Hong, B.H., Ravi, A., Chandra, B., Hone, J. and Kim, P. (2007) Scaling of Resistance and Electron Mean Free Path of Single-Walled Carbon Nanotubes. *Physical Review Letters*, **98**, 186808. <https://doi.org/10.1103/PhysRevLett.98.186808>
- [6] Kane, C.L., Mele, E.J., Lee, R.S., Fischer, J.E., Petit, P., Dai, H., Thess, A., *et al.* (1998) Temperature-Dependent Resistivity of Single-Wall Carbon Nanotubes. *EPL (Europhysics Letters)*, **41**, 683. <https://doi.org/10.1209/epl/i1998-00214-6>
- [7] Twum, A., Mensah, S.Y., Edziah, R. and Arthur, A. (2020) Laser Induced Resistivity of Chiral Single Wall Carbon Nanotubes. *Journal of Physics Communications*, **4**, 075011. <https://doi.org/10.1088/2399-6528/aba1d4>
- [8] Mensah, S.Y. and Kangah, G.K. (1992) The Thermoelectric Effect in a Semiconductor Superlattice in a Non-Quantized Electric Field. *Journal of Physics: Condensed Matter*, **4**, 919. <https://doi.org/10.1088/0953-8984/4/3/031>
- [9] Slepyan, G.Y., Maksimenko, S.A., Lakhtakia, A., Shenko, O.M.Y. and Gusakov, A.V. (1998) Electronic and Electromagnetic Properties of Nanotubes. *Physical Review B*, **57**, 9485. <https://doi.org/10.1103/PhysRevB.57.9485>

- [10] Yevtushenko, O.M., Slepyan, G.Y., Maksimenko, S.A., Lakhtakia, A. and Romanov, D.A. (1997) Nonlinear Electron Transport Effects in a Chiral Carbon Nanotube. *Physical Review Letters*, **79**, 1102. <https://doi.org/10.1103/PhysRevLett.79.1102>
- [11] Mensah, S.Y., Allotey, F.K.A., Mensah, N.G. and Nkrumah, G. (2001) Differential Thermopower of a CNT Chiral Carbon Nanotube. *Journal of Physics: Condensed Matter*, **13**, 5653. <https://doi.org/10.1088/0953-8984/13/24/310>
- [12] Vavro, J., Kikkawa, J.M. and Fischer, J.E. (2005) Metal-Insulator Transition in Doped Single-Wall Carbon Nanotubes. *Physical Review B*, **71**, 155410. <https://doi.org/10.1103/PhysRevB.71.155410>
- [13] Yanagi, K., Udoguchi, H., Sagitani, S., Oshima, Y., Takenobu, T., Kataura, H., Ishida, T., Matsuda, K. and Maniwa, Y. (2010) Transport Mechanisms in Metallic and Semiconducting Single-Wall Carbon Nanotube Networks. *Acs Nano*, **4**, 4027-4032. <https://doi.org/10.1021/nn101177n>